

Article

# RF Magnetron Sputtering Deposition of TiO<sub>2</sub> Thin Films in a Small Continuous Oxygen Flow Rate

Octavian-Gabriel Simionescu <sup>1,2,\*</sup>, Cosmin Romanițan <sup>1,2</sup>, Oana Tutunaru <sup>1</sup>, Valentin Ion <sup>3</sup>, Octavian Buiu <sup>1</sup> and Andrei Avram <sup>1</sup>

<sup>1</sup> National Institute for Research and Development in Microtechnologies, 126A Erou Iancu Nicolae Street, Voluntari City, Ilfov County, 077190 Bucharest, Romania

<sup>2</sup> Faculty of Physics, University of Bucharest, 405 Atomistilor Street, Magurele city, Ilfov County, 077125 Bucharest, Romania

<sup>3</sup> National Institute for Laser, Plasma and Radiation Physics, 409 Atomistilor Street, Magurele City, Ilfov County, 077125 Bucharest, Romania

\* Correspondence: octavian.simionescu@imt.ro

Received: 21 May 2019; Accepted: 12 July 2019; Published: 16 July 2019



**Abstract:** Rutile titanium oxide (TiO<sub>2</sub>) thin films require more energy to crystallize than the anatase phase of TiO<sub>2</sub>. It is a prime candidate for micro-optoelectronics and is usually obtained either by high substrate temperature, applying a substrate bias, pulsed gas flow to modify the pressure, or *situ* annealing. In the present work, we managed to obtain high enough energy at the substrate in order for the particles to form rutile TiO<sub>2</sub> at room temperature without any intentional substrate bias in a continuous gas flow. The rutile TiO<sub>2</sub> thin films were deposited by a reactive radiofrequency magnetron sputtering system from a titanium target, in an argon/oxygen gas mixture. Investigations regarding the film's structure and morphology were performed by X-ray diffraction (XRD), X-ray reflectivity (XRR), scanning electron microscopy (SEM) and energy-dispersive X-ray spectroscopy (EDAX), while the optical properties were investigated by means of ellipsometry.

**Keywords:** room temperature; magnetron sputtering; rutile TiO<sub>2</sub>

## 1. Introduction

Titanium dioxide (TiO<sub>2</sub>) thin films play a significant role in different areas of research and may lead to promising applications, due to its very good optical and electrical properties, high chemical stability and non-toxic nature. Over the years, TiO<sub>2</sub> has been studied for many potential applications, including as a coating for self-cleaning surfaces, the white pigment in paints and food coloring, solar cells [1], biomaterials applications [2,3], as a material for corrosion resistance [4–10], and gas sensing [11,12]. TiO<sub>2</sub> can be deposited through various methods [13] such as chemical vapor deposition (CVD), pulsed laser deposition (PLD), electrophoretic deposition (EPD), magnetron sputtering (MS), and sol-gel dip-coating. Magnetron sputtering provides many advantages, like very good adhesion, fast deposition rates and good control of the film structure.

However, in nature, TiO<sub>2</sub> can be found in three forms: brookite, which has an orthorhombic structure with the spatial group *Pbca*; and two tetragonal structures—rutile (*P4<sub>2</sub>/mnm*) and anatase (*I4<sub>1</sub>/amd*). In the thin film industry, the rutile and anatase phases are the most commonly used, each of them having different advantages over the other. TiO<sub>2</sub> has a refractive index of  $n \approx 1.7$ –2.7 [1,14], rutile having a higher  $n$  (~2.7) than anatase [15]. Rutile also presents a higher dielectric constant, sometimes reaching 63 [16], compared to anatase, which has a dielectric constant of 6–19 [17]. However, anatase has a wider optical band gap than rutile (3.2 eV vs. 3.0 eV, respectively) [14]. In this context,

rutile is a promising candidate for filters, dielectric mirrors of lasers and optical anti-reflective thin layers [18], while anatase is more desired in photocatalytic applications [13,19–21].

In reactive magnetron sputtering, titanium (Ti) is sputtered from a metallic target by energetic ions of a noble gas. By supplying a reactive gas to the chamber, TiO<sub>2</sub> can be formed and deposited onto a chosen substrate. MS deposition of TiO<sub>2</sub> is highly dependent on the energy at the substrate and the deposition of crystalline TiO<sub>2</sub>, especially in the rutile phase, usually requires either a substrate bias voltage, a very high substrate temperature or a combination of both. To avoid using a high substrate temperature, high power impulse magnetron sputtering (HiPIMS) can also be used as an alternative [15,22]. The goal is to increase the energy of the incident ions, as rutile requires higher energy to crystallize than anatase [23–25]. This can be seen in the work of Nezar et al. where, without any substrate bias, the deposited films consisted of anatase TiO<sub>2</sub>, and only after the application of a –75 V substrate bias could the peak for the rutile phase be noticed in XRD analysis [26].

In this work, the structural, morphological and optical properties of TiO<sub>2</sub> thin films deposited at different oxygen flow rates have been investigated. We show that it is possible to obtain crystalline, homogeneous TiO<sub>2</sub> thin films with smooth surfaces (roughness of 0.2% of the total thickness) on silicon substrates by radiofrequency (RF) MS, without applying any substrate bias voltage at room temperature (RT).

## 2. Materials and Methods

### 2.1. Substrate Preparation

The TiO<sub>2</sub> thin films were reactively sputtered on P/Boron-doped silicon substrates with (100) crystallographic orientation, 1–10 Ω/cm resistivity and a 525 ± 25 μm thickness. Prior to the depositions, the 100 mm diameter p-Si wafers were diced into 1.7/1.7 cm pieces with a diamond disk so the depositions can be made under different parameters. The pieces were washed in an ultrasound bath with Extran<sup>®</sup> (Merk GaA, Darmstadt, Germany) detergent for 10 min and after that in a piranha solution (H<sub>2</sub>SO<sub>4</sub>:H<sub>2</sub>O = 3:1).

### 2.2. Deposition Parameters

The depositions were performed with a RF magnetron sputtering PlasmalabSystem400 (Oxford Instruments, Abingdon, UK) using the parameters described in Table 1. The sputtering was made from a titanium target with a 150 mm diameter and 6 mm thickness, attached to a balanced magnetron. The substrate holder was cooled with water to keep the substrate temperature at room value and we have not applied an electrical potential over the substrate in order to induce a desired bias, the substrate holder being grounded. The temperature was measured in real time by a built-in thermocouple. Argon (Ar) and molecular oxygen (O<sub>2</sub>) were used as sputtering and reactive gases respectively. The flow rate of the respective gases was monitored individually by 1179A mass flow controllers using a closed loop system. A base pressure of 1.33 × 10<sup>–5</sup> Pa is reached by an Alcatel ATH500M (Pfeiffer Vacuum, Aßlar, Germany) turbo pump backed by an Alcatel ACP40G dry pump and monitored by an active Penning gauge. The process pressure is controlled by a sealable modulating gate valve placed between the chamber and the turbo-molecular pump and monitored by a 100 mTorr CM gauge. The substrate oscillates under the target for 26.6 min, by a 30° angle and a period of 7.98 s per oscillation, for the purpose of uniformity. With these parameters, the obtained TiO<sub>2</sub> thin films usually grow ~30 nm thick with a deposition rate of ~1.2 nm/min.

**Table 1.** Deposition parameters for the TiO<sub>2</sub> films.

Parameter	Value
Target	Ti (99.5% pure)
Target-to-substrate distance (mm)	90
Base pressure (Pa)	$1.33 \times 10^{-5}$
Process pressure (Pa)	0.26
RF power (W)	500
RF power target density <sup>1</sup> (W/cm <sup>2</sup> )	2.83
Argon flow rate (sccm <sup>2</sup> )	30 (99.999% pure)
Oxygen flow rate (sccm)	0–2 (0.5 step) (99.999% pure)

<sup>1</sup> value was averaged over the whole target area; <sup>2</sup> sccm = standard cubic centimeter per minute.

### 2.3. Characterization Techniques

To determine the crystallization phases, we used a SmartLab diffraction system (Rigaku Corporation, Tokyo, Japan) with CuK $\alpha_1$  wavelength (1.5406 Å) in Grazing Incidence (GI-XRD) mode using an incidence angle of 0.5°. The phase identification was made by referring to the International Center for Diffraction Data (ICDD) database.

The structural parameters were determined using Rietveld analysis, which allowed us to analyze simultaneously both lattice strain and mean crystallite size. The small values of the fitting parameters ( $R$  and  $\chi^2$ ) assure us of the accuracy of the obtained results. Moreover, we used X-ray reflectivity (XRR) to calculate thickness, density and roughness. The XRR results obtained for the investigated films were simulated with the parallel tempering algorithm of the GlobalFit (Rigaku Corporation, Tokyo, Japan) integrated thin film analysis software (Version 2.0.5.2).

SEM and EDAX were used to characterize the surface morphology, film thickness and composition of the TiO<sub>2</sub> samples. The surface morphology and thickness of the TiO<sub>2</sub> samples were acquired with a Nova NanoSEM 630 Scanning Electron Microscope (FEI Company, Hillsboro, OR, USA) using UHR detector (Through-Lens-Detector-TLD) at an acceleration voltage of 10 kV.

The distribution of the chemical constituents of interest within the TiO<sub>2</sub> samples was performed with the element energy dispersive spectroscopy (EDS) system (Smart Insight AMETEK). The EDAX map was acquired at an acceleration voltage of 6 kV, with a working distance of 5 mm and 2000 $\times$  magnification.

The spectroscopic ellipsometry measurements were made using a V-Vase spectroellipsometer (J.A. Woollam Co., Lincoln, NE, USA) equipped with a HS-190 monochromator with xenon discharge lamp. The experimental values of  $\Psi$  (amplitude ratio) and  $\Delta$  (phase difference) were taken in the spectral range of 300–1700 nm (0.72–4.13 eV) with a step of 2 nm and at 60°, 65° and 70° angles of incidence. To extract the thickness, the roughness and the optical constants of our samples we built an optical model consisting of four layers: Silicon substrate, native silicon oxide (~3 nm), a thin layer of TiO<sub>2</sub>, and a top rough layer. The dielectric function for silicon and native silicon oxide was taken from the literature [27]. The top rough layer was considered to be a mixture of TiO<sub>2</sub> and voids ( $n \sim 1$ ) in Bruggeman approximation [28]. The difference between our chosen model and the experimental data is given by MSE (mean square error) values:

$$MSE = \frac{1}{2N - M} \sum_{i=1}^n \left[ \left( \frac{\Psi_i^{mod} - \Psi_i^{exp}}{\sigma_{\Psi_i}^{exp}} \right)^2 + \left( \frac{\Delta_i^{mod} - \Delta_i^{exp}}{\sigma_{\Delta_i}^{exp}} \right)^2 \right], \quad (1)$$

where  $N$  is the number of ( $\Psi$ ,  $\Delta$ ) pairs,  $M$  is the number of variable parameters in the model, and  $\sigma$  is the standard deviation on the experimental data points.

The fitting procedure consists of three steps. In the first step, the thickness of the TiO<sub>2</sub> layer and that of the top rough layer was calculated using a simple Cauchy dispersion in the wavelength range of 500–1700 nm, where the thin films are transparent. In the second step, the Cauchy dispersion was

replaced with a single Gauss oscillator which is fully Kramer–Kronig consistent. This step is necessary to calculate the optical constants in high absorption range, due to the limitations of the Cauchy dispersion [28], and to decrease the MSE value, the smallest value representing the best fit. Figure 1 presents an example of a fit result for a TiO<sub>2</sub> thin film deposited on a Si substrate at Ar:O<sub>2</sub> = 30:1.5 sccm flow rate. The presented result is obtained from fitting with a single Gauss oscillator. As can be seen, the generated data of Ψ (Figure 1a) and Δ (Figure 1b) and the experimental data match, confirming that our optical model is accurate.

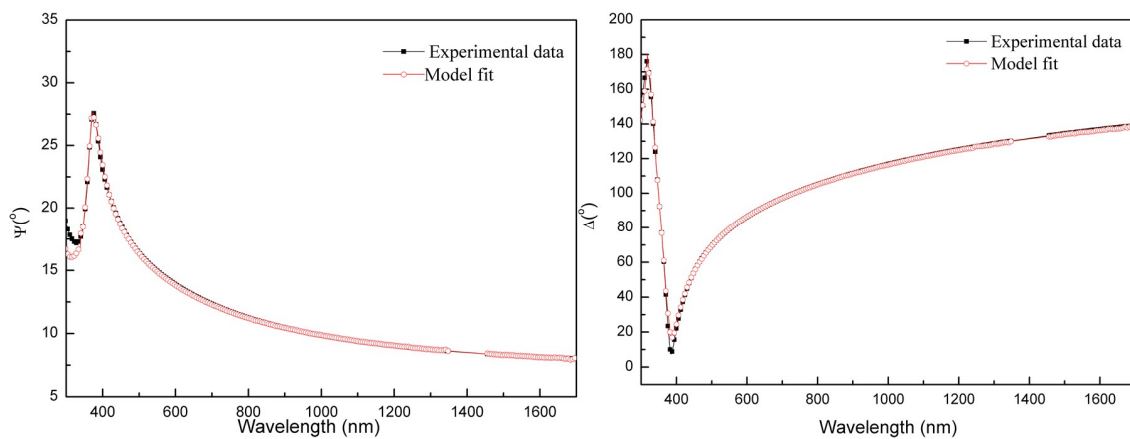


**Figure 1.** Experimental data for a TiO<sub>2</sub> thin film deposited at Ar:O<sub>2</sub> flow rate of 30:1.5 sccm vs. the model fit with a single Gauss oscillator for (a) the amplitude ratio Ψ, and (b) the phase difference Δ.

In the third step, in order to minimize the values of MSE, the parameters of the oscillator were slightly adjusted and are presented in Table 2. After this step, we could extract the final values of film thickness, surface roughness, refractive index and extinction coefficient.

**Table 2.** The values of Gauss parameters and MSE obtained by fitting the experimental data with a single oscillator.

Ar:O <sub>2</sub> Flow (sccm)	Amp	E <sub>n</sub> (eV)	B <sub>r</sub> (eV)	E <sub>inf</sub> <sup>1</sup>	MSE
30:1	20.852 ± 0.0704	4.5444 ± 0.0062	0.91657 ± 0.00601	3.1789 ± 0.0236	6.552
30:1.5	19.369 ± 0.075	4.5151 ± 0.00603	0.92139 ± 0.00632	3.3776 ± 0.0325	7.901
30:2	19.411 ± 0.0736	4.4924 ± 0.00634	0.90886 ± 0.00628	3.3995 ± 0.0271	7.79

<sup>1</sup> The third decimals for the absolute errors result from software calculation. A single decimal is more reasonable.

The parameters presented in Table 2 are the Gauss parameters. The total dielectric function is given by

$$\epsilon = \epsilon_1 + i\epsilon_2 = e_{1offset} + \epsilon_{n-Gauss}, \tag{2}$$

where e<sub>1offset</sub> is a purely real constant, equivalent to ε<sub>inf</sub>, and

$$\epsilon_1 = \epsilon_{inf} + \frac{2}{\pi} P \int_{E_g}^{\infty} \frac{\xi \epsilon_2(\xi)}{\xi^2 - E^2} d\xi \tag{3}$$

$$\epsilon_2 = A_n e^{-\left(\frac{E-E_n}{\sigma}\right)^2} - A_n e^{-\left(\frac{E+E_n}{\sigma}\right)^2} \tag{4}$$

$$\sigma = \frac{Br_n}{2\sqrt{\ln(2)}} \tag{5}$$

where  $A_n$  (Amp in Table 2) is the amplitude of oscillation (dimensionless),  $E_n$  is the center energy and  $Br$  is the broadening of the absorption peak;  $\varepsilon_1$  and  $\varepsilon_2$  are the real and the imaginary part of the dielectric function and  $\varepsilon_{inf}$  is the value of the dielectric constant at infinity [28].

### 3. Results

When no oxygen was supplied to the reaction chamber, the (100), (002), (101) and (102) crystal planes of titanium (Ti-PDF No. 900-8517) can be observed at  $2\theta$  diffraction angles of  $35.09^\circ$ ,  $38.33^\circ$ ,  $40.11^\circ$  and  $53.04^\circ$ , respectively. In Figure 2, it can be noticed that by introducing a small amount of oxygen, insufficient to reactively form  $\text{TiO}_2$  with the titanium, the peak positions are shifted to smaller values ( $34.78^\circ$ ,  $37.86^\circ$ ,  $39.94^\circ$  and  $52.47^\circ$ ). This fact is related to the increase of the titanium lattice constant, which also implies an additional lattice strain of  $\sim 0.4\%$ . Moreover, we can see a peak broadening after the oxygen incorporation, indicating a decrease of the mean crystallite size from 11.4 to 4.93 nm, according to Rietveld analysis.

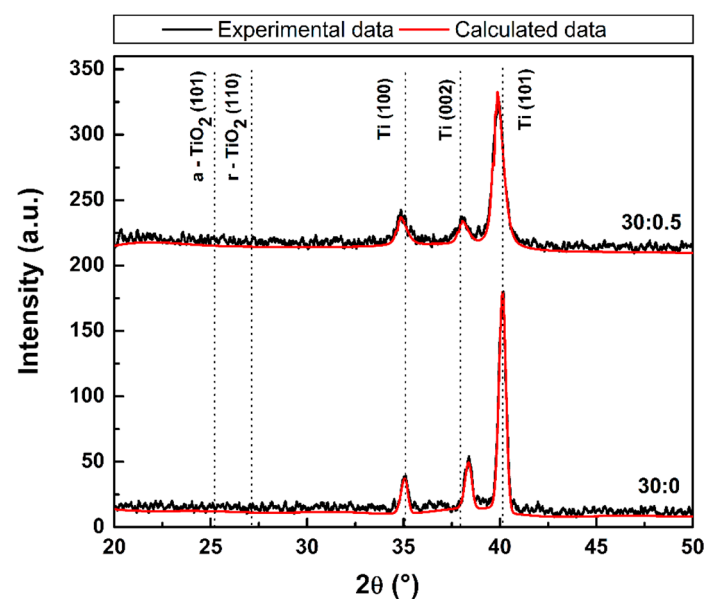


**Figure 2.** Experimental GI-XRD pattern of a Ti thin film deposited under Ar:O<sub>2</sub> = 30:0 sccm flow rate (bottom) and Ar:O<sub>2</sub> = 30:0.5 sccm flow rate (top) in the chamber (black curves) and simulated patterns (red curves).

By increasing the oxygen flow rate, we successfully deposited  $\text{TiO}_2$  thin films in the rutile phase with multiple crystal orientations: (110), (101), (200), (210), (211), (220), (002) and (301), according to PDF No. 900-7432. The main diffraction feature located at  $27.16^\circ$ , corresponds to the (110) atomic plane, while the secondary diffraction features from  $53.57^\circ$  and  $55.49^\circ$  correspond to the (211) and (220) atomic planes, respectively (Figure 3).

To gain a deeper understanding of the structural parameters, we refined each pattern using Rietveld analysis (red curve). Accordingly, the  $\text{TiO}_2$  phase was identified and the mean crystallite size and lattice strain were determined. Clearly, the predominant peak is that of the rutile phase (110), found at  $27.16^\circ$ , for all  $\text{TiO}_2$  samples. Furthermore, it can be observed that the diffraction features located at  $25.28^\circ$  and  $49.25^\circ$  were not resolved with the Rietveld analysis for the rutile phase. These features are attributed to the (101) and (002) crystal orientations of the anatase phase, respectively, according to PDF No. 001-0562. In this framework, the final result consists of a mixture of rutile and anatase, where the percentage of the latter is under 5%. The structural parameters for Ti and  $\text{TiO}_2$ , extracted from the Rietveld analysis, are listed in Table 3.

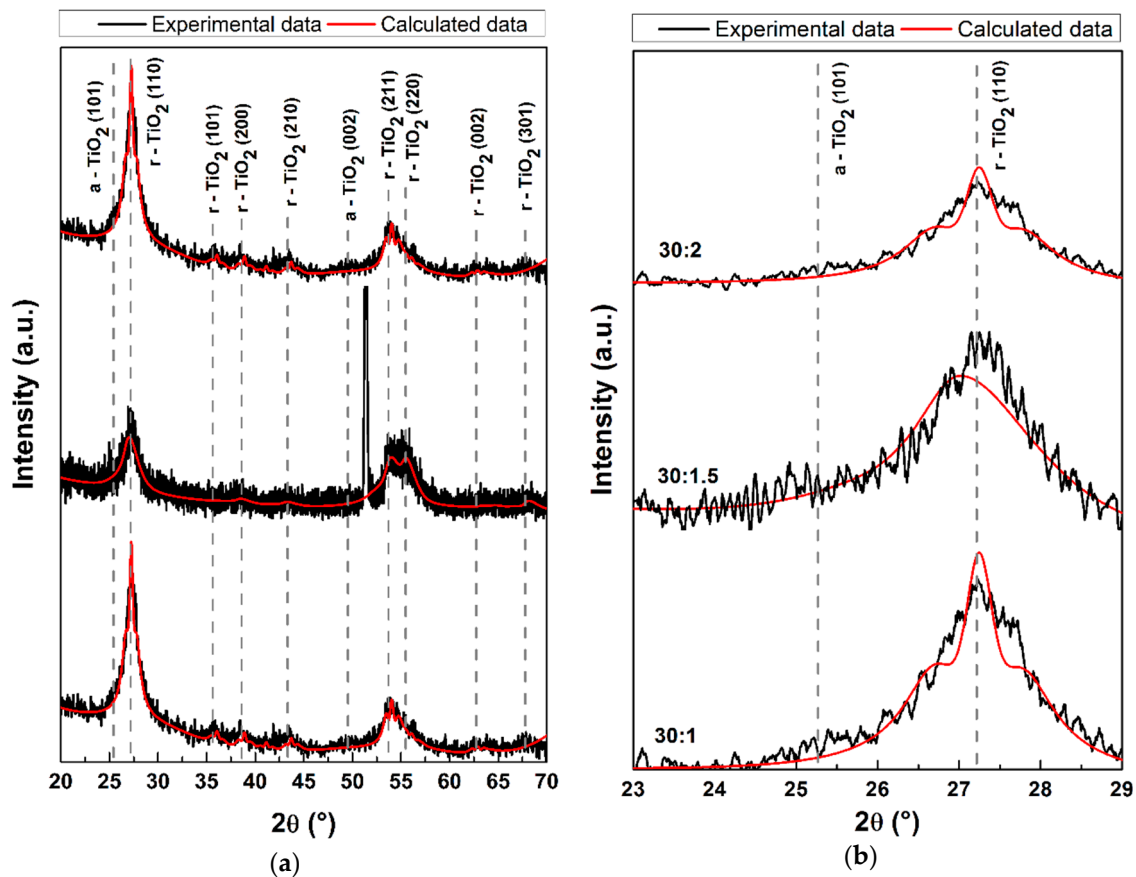


**Figure 3.** (a) Experimental GI-XRD patterns (black curve) of the investigated samples and the corresponding simulated curves (red curve). The letters “r” and “a” symbolize the rutile and anatase phases and the sharp peak at  $\sim 51^\circ$  for the middle spectrum (Ar:O<sub>2</sub> = 30:1.5) is caused by the Si substrate. (b) Enhancement of (a) in the  $2\theta$  range of  $23^\circ$ – $29^\circ$  for the TiO<sub>2</sub> thin films.

**Table 3.** Structural parameters for Ti and TiO<sub>2</sub>: lattice constant, lattice strain and mean crystallite size.

Ar:O <sub>2</sub> Flow (sccm)	Lattice Constant (nm)			Lattice Strain (%)	Mean Crystallite Size (nm)
	a	b	c		
30:0	0.29	0.29	0.46	0.15	11.4
30:0.5	0.30	0.30	0.47	0.44	4.9
30:1	0.46	0.46	0.29	0.67	4.3
30:1.5	0.46	0.46	0.29	0.55	3.1
30:2	0.46	0.46	0.29	0.61	3.7

Contrary to the Ti phase, the TiO<sub>2</sub> one exhibits the same lattice constant among different Ar:O<sub>2</sub> flow rates. It can be remarked that on one hand, the lattice strain increases significantly (reaching four-fold higher values) and, on the other hand, the mean crystallite size suffers a strong decrease for the different Ar:O<sub>2</sub> flow rates. XRR measurements were performed in order to study thickness, density and surface roughness of the deposited thin films. The parameters from the insets in Figure 4 were obtained after the fitting of the experimental X-ray profiles (black curves), accounting for a multilayer structure TiO<sub>2</sub>/SiO<sub>2</sub>/Si.

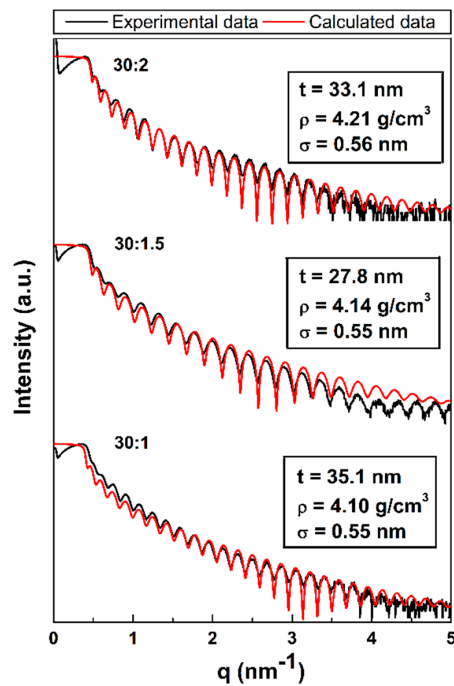


**Figure 4.** XRR profiles and calculated data. Inset represents thickness ( $t$ ), density ( $\rho$ ) and surface roughness ( $\sigma$ ).

It can be observed that the density is close to the theoretical value for  $\text{TiO}_2$  ( $4.23 \text{ g/cm}^3$ ) and the roughness is very small ( $\sim 0.2\%$  of the total thickness) for all investigated samples. The obtained thicknesses are also supported by the cross-sectional SEM micrographs (Figure 5) and the spectroscopic ellipsometry results. The technological impact of this, would be the opportunity of obtaining dense thin films with a very smooth surface and with a small crystallite size.

From the SEM analysis we can see that our films are continuous, presenting no nano- or micro-fissures. The thicknesses obtained from the cross-section represented in Figure 5 are of  $\sim 35$ , 28 and 33 nm for the  $\text{TiO}_2$  film deposited at  $\text{Ar:O}_2 = 30:1$ ,  $30:1.5$  and  $30:2$  sccm flow rate, respectively. Seeing that our samples are extremely thin, we acquired the SEM micrographs at 300 kx magnification. It can prove to be difficult to obtain a very high resolution at this magnification, as we are approaching our measuring apparatus' limits. Nevertheless, the micrographs in Figure 5 appear to show a highly dense microstructure.

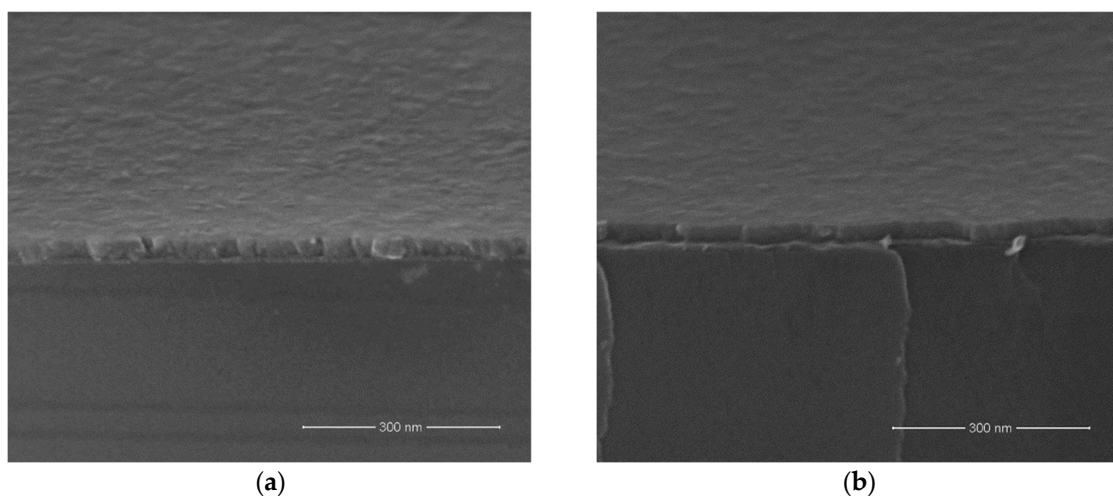
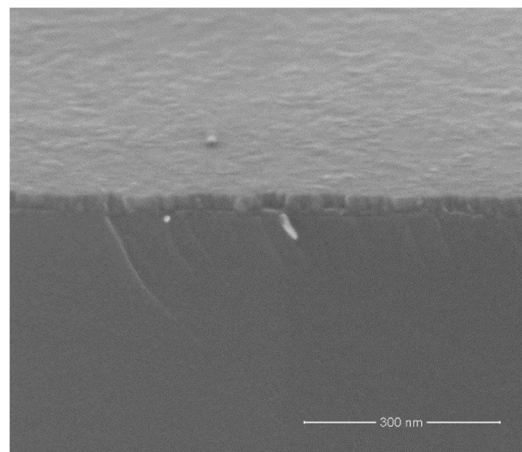


**Figure 5.** Cont.



(c)

**Figure 5.** Cross-section SEM images at 300 k $\times$  magnification of TiO<sub>2</sub> film deposited at (a) Ar:O<sub>2</sub> = 30:1, (b) Ar:O<sub>2</sub> = 30:1.5 and (c) Ar:O<sub>2</sub> = 30:2 sccm flow rate.

Besides the features caused by the splitting of the films in order to prepare them for SEM cross-section analysis, our samples appear to be featureless, or at least fibrous. This information [29,30], together with the film's shiny gold color [31], the low process pressure and  $T/T_m$  ratio we used, where  $T$  is the substrate temperature and  $T_m = 1870$  °C is the melting temperature for TiO<sub>2</sub> [32], would classify all the present deposited TiO<sub>2</sub> thin films in zone T of Thornton's structure zone model (SZM) for sputter deposition films [33].

The distribution of the chemical constituents of interest within the TiO<sub>2</sub> samples was revealed by EDAX mapping at 2000 $\times$  magnification. From the EDAX mapping, we notice that the titanium and oxygen atoms are uniformly spread across the surface with a ratio of O:Ti  $\approx$  2.1:1 (Figure 6).

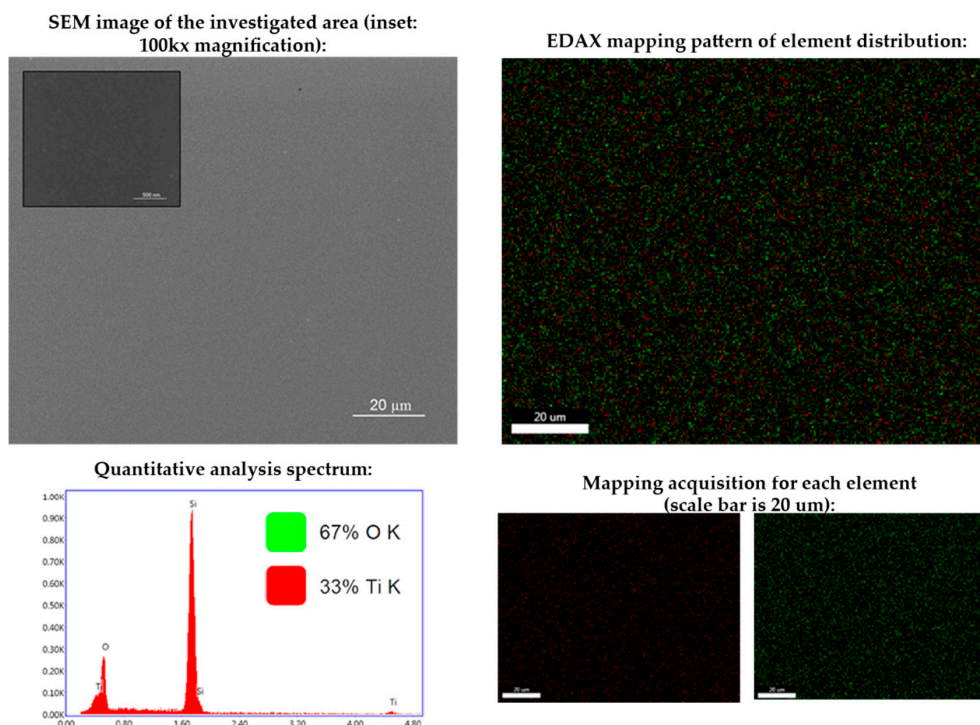


**Figure 6.** Element distribution mapping at 2000 $\times$  magnification of the TiO<sub>2</sub> sample deposited under Ar:O<sub>2</sub> = 30:2 sccm flow rate.

By fitting the experimental data from our spectroscopic ellipsometry measurements with a single Gauss oscillator, we obtained thickness values in the range of 28–36 nm with a roughness of ~1 nm for all the TiO<sub>2</sub> samples, which is in accordance with our XRR and SEM findings.

Since the O<sub>2</sub> flow varied in very small increments, the optical constants are very similar for all our TiO<sub>2</sub> samples, which can be observed in Figure 7. The refractive index varies between the different TiO<sub>2</sub> thin films just from the third decimal on, having a value of  $n = \sim 2.65$  at a wavelength of  $\lambda = 550$  nm. Values of  $n = 2.57$  and  $n = 2.74$ , at  $\lambda = 550$  nm, were reported by Tanemura et al. [34] for RF-MS-deposited anatase and rutile TiO<sub>2</sub>, respectively. This result further confirms our initial analysis from the X-ray diffractograms—that our films consist of a mixture of the anatase and the rutile phase. The extinction coefficient seems to be directly proportional with the O<sub>2</sub> flow rate, the higher values being obtained for Ar:O<sub>2</sub> = 30:2 sccm flow rate. There was no optical absorption observed in the wavelength range of 400–1700 nm for either of our deposited TiO<sub>2</sub> thin films.

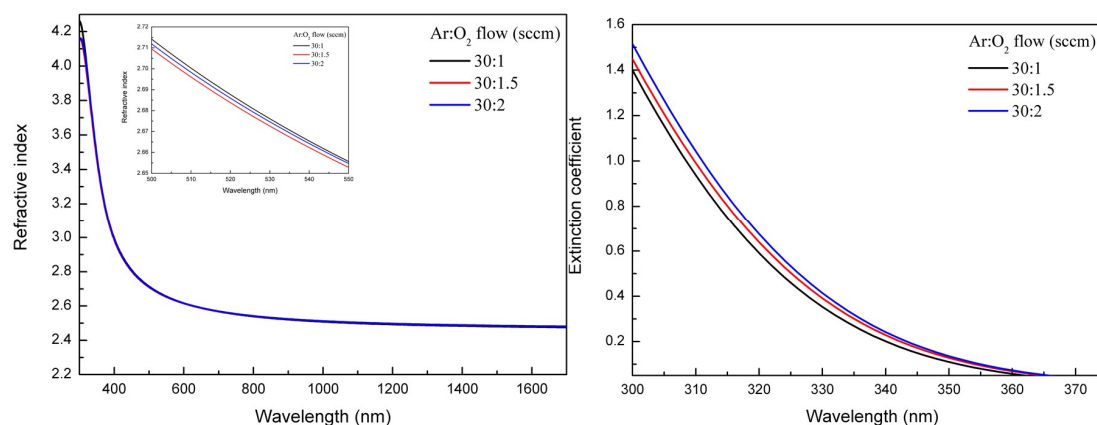


**Figure 7.** The dispersion of optical constants: (a) Refractive index (inset: enhancement in the wavelength range of 500–550 nm) and (b) extinction coefficient for the as-deposited TiO<sub>2</sub> thin films obtained from fitting with a single Gauss oscillator.

The optical band gap energy ( $E_g$ ) was extracted from the Tauc plots of  $(\alpha E)^{1/2}$  with respect to the photon energy, for indirect transitions. We obtained a band gap of  $E_g = 3.31$  eV in the case of 2 sccm O<sub>2</sub> flow rate (Figure 8), and as the O<sub>2</sub> flow rate decreases to 1.5 sccm and 1 sccm, the band gap increases to 3.4 and 3.9 eV, respectively. The very small crystallite size derived from the Rietveld analysis tells us that we have a high defect density, which would explain the high  $E_g$  values resulted from the Tauc plots, and by plotting the dependency of the optical band gap energy on the O<sub>2</sub> flow (Figure 8-inset) we can conclude that the high  $E_g$  values are due to oxygen vacancies in the TiO<sub>2</sub> lattice.

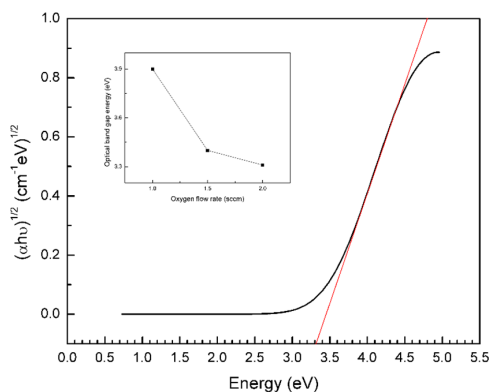


**Figure 8.** Tauc plot for indirect transitions for a TiO<sub>2</sub> thin film deposited under Ar:O<sub>2</sub>=30:2 sccm flow rate. Inset represents the plot of the optical band gap energy as a function of O<sub>2</sub> flow rate during deposition.

#### 4. Discussion

In previous works, TiO<sub>2</sub> depositions, either by RF [2] or DC [17,35] magnetron sputtering, were amorphous in continuous gas flow, if no bias voltage or heating was applied to the substrate. Crystalline TiO<sub>2</sub> (anatase, rutile or a mixture of both) was obtained either by controlling the O<sub>2</sub> flow and sputtering pressure [36,37], by applying a substrate bias voltage [3,17,38], or by annealing [39–41]. Nezar et al. [26] managed to obtain crystalline TiO<sub>2</sub> by reactive magnetron sputtering without applying any substrate bias at RT, with predominantly anatase phase (Table 4). The reason for obtaining anatase TiO<sub>2</sub>, as is the case for annealing amorphous TiO<sub>2</sub> [39–41], is that it requires less energy to form than the rutile phase. In the absence of substrate bias or heating, it is needed to adapt the other process parameters in order for the deposited particles to have enough energy to crystallize, otherwise the deposited thin film will be amorphous [42].

**Table 4.** Comparison between TiO<sub>2</sub> deposited by RF magnetron sputtering at RT and without any intentional substrate bias.

	Present Work	Nezar et al. [26]
RF power (W)	500	250
Process pressure (Pa)	0.26	2.66
O <sub>2</sub> (%)	0–6.25	25
Target-to-substrate distance (mm)	90	30
Crystallization phase	rutile	anatase
Main crystal orientation	(110), (211) and (220)	(101)

Each of the deposition parameters has an influence on the energy of the deposition particles and we have to take into consideration the geometry of the deposition chamber as well. Oxygen partial pressure can influence the deposition mode (metal/oxide)/poisoning degree of the target [36]. Deposition pressure can influence the degree of ionization and the mean free path of sputtering and deposition atoms/ions. Substrate temperature has a role in activating the surface and allowing adatoms to diffuse and occupy the vacancies in the film. Substrate bias also influences the diffusion of adatoms not only by the surface diffusion energy, but also by increasing the kinetic energies of incoming ions [3,38]. The power of the discharge plays a big part as well: By increasing it to a certain point we can maximize the sputtering yield. Keep in mind that too much power can lead to ion implantation, which is to be avoided [43]. Musil et al. [25] explained very well from where the total energy ( $E_T$ ) at the substrate comes from (Equation (6)) and how each individual term is influenced by the process parameters:

$$E_T = E_S(T_S, t_d) + E_p(U_S, i_S, p_T, a_D, t_d) + E_{mt}(W_t, d_{s-t}, t_d) + E_{ch}(t_d) + E_{rad}(t_d), \quad (6)$$

where  $E_S$  represents the heat from the substrate and is dependent on the substrate temperature ( $T_S$ ) and the deposition time ( $t_d$ );  $E_p$  represents the kinetic energy of the bombarding and fast condensing particles, and is dependent on the substrate bias ( $U_S$ ) and ion current density ( $i_S$ ), the process total pressure ( $p_T$ ) and the deposition rate ( $a_D$ ) and time;  $E_{mt}$  represents the heat incoming from the magnetron target and is dependent on the target power density ( $W_t$ ), the substrate-to-target distance ( $d_{s-t}$ ) and the deposition time;  $E_{ch}$  is the energy emanated from the exothermal chemical reactions and it has a dependency on the deposition time;  $E_{rad}$  represents the heat which is radiated from the plasma and is dependent on the deposition time. In a deposition at RT, such as the one in this study,  $E_p$  becomes the main contributor to the energy delivered to the growing film, which in turn is influenced by other process parameters, like total pressure and deposition rate. For an in-depth analysis of each term of Equation (6), please see [25].

All of the above mentioned parameters need to be fine-tuned because higher values do not always mean better results and the total amount of energy that goes into the growing thin film also

influences its later crack resistance [29,30]. Clearly, through the combination of parameters used here, the energy delivered to our growing TiO<sub>2</sub> thin films was enough to produce the rutile phase of TiO<sub>2</sub>. The influence of different combinations of these parameters can be seen in the different results obtained in other works.

## 5. Conclusions

In this work, we successfully deposited crystalline, homogeneous, rutile TiO<sub>2</sub> thin films with smooth surfaces by RF MS at RT, without any induced substrate bias and in a continuous gas flow. Nezar et al. [26] similarly did not use any substrate bias or heating and they obtained predominantly anatase TiO<sub>2</sub>. This is easily explained by the fact that we used more RF power, which increased our sputtering yield, and a considerably higher vacuum, which increased the mean free path of our atoms/ions. These, together with a very low deposition rate, are the main reasons we managed to obtain higher energy particles at the substrate.

As this work proves the possibility of depositing highly energetic TiO<sub>2</sub> by RF MS at RT, the next step would be to optimize the oxygen partial pressure in order to lower the defect density and to undertake targeted research for the possible applications of our TiO<sub>2</sub> films in micro-optoelectronics. As our samples find themselves in zone T of the SZM, they were assumed to be crack resistant [29,30] and no further tests were made. In future research, thicker films will be deposited to better analyze the cross-section microstructure and direct measurements of crack resistance will be made.

**Author Contributions:** Conceptualization, O.-G.S., O.B. and A.A.; Validation, O.B. and A.A.; Formal Analysis, O.-G.S., C.R., O.T. and V.I.; Investigation, O.-G.S., C.R., O.T. and V.I.; Resources, A.A.; Data Curation, O.-G.S.; Writing—Original Draft Preparation, O.-G.S.; Writing—Review and Editing, O.-G.S., C.R., O.T., V.I., O.B. and A.A.; Visualization, O.-G.S., C.R. and O.T.; Supervision, O.B. and A.A.; Project Administration, O.B. and A.A.; Funding Acquisition, O.B. and A.A.

**Funding:** This research was funded by the Romanian Ministry of Research and Innovation, through the contract “Advanced new research in micro/nanoelectronics, photonics and micro/nano-bio systems for applications development in the fields of specialization” (MICRO-NANO-SIS PLUS), project “Atomically thin (2D) materials and their applications at the limit of Moore’s law” (PN-19160202).

**Conflicts of Interest:** The authors declare no conflict of interest.

## References

1. Richards, B. Single-material TiO<sub>2</sub> double-layer antireflection coatings. *Sol. Energy Mater. Sol. Cells* **2003**, *79*, 369–390. [[CrossRef](#)]
2. Majeed, A.; He, J.; Jiao, L.; Zhong, X.; Sheng, Z. Surface properties and biocompatibility of nanostructured TiO<sub>2</sub> film deposited by RF magnetron sputtering. *Nanoscale Res. Lett.* **2015**, *10*, 91. [[CrossRef](#)]
3. Bait, L.; Azzouz, L.; Saoula, N.; Madaoui, N. Influence of substrate bias voltage on the properties of TiO<sub>2</sub> deposited by radio-frequency magnetron sputtering on 304L for biomaterials applications. *Appl. Surf. Sci.* **2017**, *395*, 72–77. [[CrossRef](#)]
4. Krishna, D.S.R.; Sun, Y. Thermally oxidised rutile-TiO<sub>2</sub> coating on stainless steel for tribological properties and corrosion resistance enhancement. *Appl. Surf. Sci.* **2005**, *252*, 1107–1116. [[CrossRef](#)]
5. Shen, G.; Chen, Y.; Lin, L.; Lin, C.; Scantlebury, D. Study on a hydrophobic nano-TiO<sub>2</sub> coating and its properties for corrosion protection of metals. *Electrochim. Acta* **2005**, *50*, 5083–5089. [[CrossRef](#)]
6. Bamoulid, L.; Maurette, M.T.; De Caro, D.; Guenbour, A.; Bachir, A.B.; Aries, L.; El Hajjaji, S.; Benoît-Marquié, F.; Ansart, F. An efficient protection of stainless steel against corrosion: Combination of a conversion layer and titanium dioxide deposit. *Surf. Coat. Technol.* **2008**, *202*, 5020–5026. [[CrossRef](#)]
7. Shan, C.; Hou, X.; Choy, K.L. Corrosion resistance of TiO<sub>2</sub> films grown on stainless steel by atomic layer deposition. *Surf. Coat. Technol.* **2008**, *202*, 2399–2402. [[CrossRef](#)]
8. Liu, T.; Zhang, F.; Xue, C.; Li, L.; Yin, Y. Structure stability and corrosion resistance of nano-TiO<sub>2</sub> coatings on aluminum in seawater by a vacuum dip-coating method. *Surf. Coat. Technol.* **2010**, *205*, 2335–2339. [[CrossRef](#)]

9. Xie, D.; Wang, H.; Ganesan, R.; Leng, Y.; Sun, H.; Huang, N. Fatigue durability and corrosion resistance of TiO<sub>2</sub> films on CoCrMo alloy under cyclic deformation. *Surf. Coat. Technol.* **2015**, *275*, 252–259. [[CrossRef](#)]
10. Wang, N.; Fu, W.; Zhang, J.; Li, X.; Fang, Q. Corrosion performance of waterborne epoxy coatings containing polyethylenimine treated mesoporous-TiO<sub>2</sub> nanoparticles on mild steel. *Prog. Org. Coat.* **2015**, *89*, 114–122. [[CrossRef](#)]
11. Karunagaran, B.; Uthirakumar, P.; Chung, S.; Velumani, S.; Suh, E.K. TiO<sub>2</sub> thin film gas sensor for monitoring ammonia. *Mater. Charact.* **2007**, *58*, 680–684. [[CrossRef](#)]
12. Dhivya, P.; Prasad, A.K.; Sridharan, M. Nanostructured TiO<sub>2</sub> films: Enhanced NH<sub>3</sub> detection at room temperature. *Ceram. Int.* **2014**, *40*, 409–415. [[CrossRef](#)]
13. Patil, M.K.; Shaikh, S.; Ganesh, I. Recent advances on TiO<sub>2</sub> thin film based photocatalytic applications (A review). *Curr. Nanosci.* **2015**, *11*, 271–285. [[CrossRef](#)]
14. Nair, P.B.; Justinictor, V.B.; Daniel, G.P.; Joy, K.; Raju, K.J.; Kumar, D.D.; Thomas, P.V. Optical parameters induced by phase transformation in RF magnetron sputtered TiO<sub>2</sub> nanostructured thin films. *Prog. Nat. Sci. Mater. Int.* **2014**, *24*, 218–225. [[CrossRef](#)]
15. Schönberger, W.; Bartzsch, H.; Schippel, S.; Bachmann, T. Deposition of rutile TiO<sub>2</sub> films by pulsed and high power pulsed magnetron sputtering. *Surf. Coat. Technol.* **2016**, *293*, 16–20. [[CrossRef](#)]
16. Wypych, A.; Bobowska, I.; Tracz, M.; Opasińska, A.; Kadlubowski, S.; Krzywania-Kaliszewska, A.; Grobelny, J.; Wojciechowski, P. Dielectric properties and characterisation of titanium dioxide obtained by different chemistry methods. *J. Nanomater.* **2014**, *2014*, 1–9. [[CrossRef](#)]
17. Sekhar, M.C.; Kondaiah, P.; Chandra, S.J.; Rao, G.M.; Uthanna, S. Effect of substrate bias voltage on the structure, electric and dielectric properties of TiO<sub>2</sub> thin films by DC magnetron sputtering. *Appl. Surf. Sci.* **2011**, *258*, 1789–1796. [[CrossRef](#)]
18. Selhofer, H.; Muller, R. Comparison of pure and mixed coating materials for AR coatings for use by reactive evaporation on glass and plastic lenses. *Thin Solid Film.* **1999**, *351*, 180–183. [[CrossRef](#)]
19. Yu, J.; Zhao, X. Effect of substrates on the photocatalytic activity of nanometer TiO<sub>2</sub> thin films. *Mater. Res. Bull.* **2000**, *35*, 1293–1301. [[CrossRef](#)]
20. Song, P.; Irie, Y.; Shigesato, Y. Crystallinity and photocatalytic activity of TiO<sub>2</sub> films deposited by reactive sputtering with radio frequency substrate bias. *Thin Solid Film.* **2006**, *496*, 121–125. [[CrossRef](#)]
21. Jagadale, T.C.; Takale, S.P.; Sonawane, R.S.; Joshi, H.M.; Patil, S.I.; Kale, B.B.; Ogale, S.B. N-Doped TiO<sub>2</sub> nanoparticle based visible light photocatalyst by modified peroxide sol–gel method. *J. Phys. Chem. C* **2008**, *112*, 14595–14602. [[CrossRef](#)]
22. Višniakov, J.; Janulevičius, A.; Maneikis, A.; Matulaitienė, I.; Selskis, A.; Stanionytė, S.; Suchodolskis, A. Antireflection TiO<sub>2</sub> coatings on textured surface grown by HiPIMS. *Thin Solid Film.* **2017**, *628*, 190–195. [[CrossRef](#)]
23. Šícha, J.; Novák, O.; Kudláček, P.; Vlček, J. Ion flux characteristics in pulsed dual magnetron discharges used for deposition of photoactive TiO<sub>2</sub> films. *Plasma Process. Polym.* **2011**, *8*, 191–199. [[CrossRef](#)]
24. Šícha, J.; Heřman, D.; Musil, J.; Stryhal, Z.; Pavlík, J. High-rate low-temperature DC pulsed magnetron sputtering of photocatalytic TiO<sub>2</sub> films: The effect of repetition frequency. *Nanoscale Res. Lett.* **2007**, *2*, 123–129. [[CrossRef](#)]
25. Musil, J.; Šícha, J.; Heřman, D.; Čerstvý, R. Role of energy in low-temperature high-rate formation of hydrophilic TiO<sub>2</sub> thin films using pulsed magnetron sputtering. *J. Vac. Sci. Technol. A* **2007**, *25*, 666. [[CrossRef](#)]
26. Nezar, S.; Sali, S.; Faiz, M.; Mekki, M.; Laoufi, N.A.; Saoula, N.; Tabet, N. Properties of TiO<sub>2</sub> thin films deposited by rf reactive magnetron sputtering on biased substrates. *Appl. Surf. Sci.* **2017**, *395*, 172–179. [[CrossRef](#)]
27. Herzinger, C.M.; Johs, B.; McGahan, W.A.; Woollam, J.A.; Paulson, W. Ellipsometric determination of optical constants for silicon and thermally grown silicon dioxide via a multi-sample, multi-wavelength, multi-angle investigation. *J. Appl. Phys.* **1998**, *83*, 3323–3336. [[CrossRef](#)]
28. Fujiwara, H. *Spectroscopic Ellipsometry Principles and Applications*; John Wiley & Sons Ltd.: West Sussex, UK, 2007; ISBN 978-0-470-01608-4.
29. Musil, J. Hard nanocomposite coatings: Thermal stability, oxidation resistance and toughness. *Surf. Coat. Technol.* **2012**, *207*, 50–65. [[CrossRef](#)]
30. Musil, J. Flexible hard nanocomposite coatings. *RSC Adv.* **2015**, *5*, 60482–60495. [[CrossRef](#)]

31. Kelly, P.J.; Arnell, R.D. Development of a novel structure zone model relating to the closed-field unbalanced magnetron sputtering system. *J. Vac. Sci. Technol. A* **1998**, *16*, 2858–2869. [[CrossRef](#)]
32. Miao, L.; Jin, P.; Kaneko, K.; Terai, A.; Nabatova-Gabain, N.; Tanemura, S. Preparation and characterization of polycrystalline anatase and rutile TiO<sub>2</sub> thin films by rf magnetron sputtering. *Appl. Surf. Sci.* **2003**, *212*, 255–263. [[CrossRef](#)]
33. Thornton, J.A. Influence of apparatus geometry and deposition conditions on the structure and topography of thick sputtered coatings. *J. Vac. Sci. Technol.* **1974**, *11*, 666–670. [[CrossRef](#)]
34. Tanemura, S.; Miao, L.; Jin, P.; Kaneko, K.; Terai, A.; Nabatova-Gabain, N. Optical properties of polycrystalline and epitaxial anatase and rutile TiO<sub>2</sub> thin films by rf magnetron sputtering. *Appl. Surf. Sci.* **2003**, *212*, 654–660. [[CrossRef](#)]
35. Sekhar, M.C.; Kondaiah, P.; Krishna, B.R.; Uthanna, S. Effect of oxygen partial pressure on the electrical and optical properties of DC magnetron sputtered amorphous TiO<sub>2</sub> films. *J. Spectrosc.* **2013**, *2013*, 1–7. [[CrossRef](#)]
36. Liao, M.; Niu, H.; Chen, G. Effect of sputtering pressure and post-annealing on hydrophilicity of TiO<sub>2</sub> thin films deposited by reactive magnetron sputtering. *Thin Solid Film.* **2010**, *518*, 7258–7262. [[CrossRef](#)]
37. Wiatrowski, A.; Mazur, M.; Obstarczyk, A.; Wojcieszak, D.; Kaczmarek, D.; Morgiel, J.; Gibson, D. Comparison of the physicochemical properties of TiO<sub>2</sub> thin films obtained by magnetron sputtering with continuous and pulsed gas flow. *Coatings* **2018**, *8*, 412. [[CrossRef](#)]
38. Zheng, J.; Bao, S.; Guo, Y.; Jin, P. TiO<sub>2</sub> films prepared by DC reactive magnetron sputtering at room temperature: Phase control and photocatalytic properties. *Surf. Coat. Technol.* **2014**, *240*, 293–300. [[CrossRef](#)]
39. Nair, P.B.; Justinivictor, V.; Daniel, G.P.; Joy, K.; Ramakrishnan, V.; Thomas, P. Effect of RF power and sputtering pressure on the structural and optical properties of TiO<sub>2</sub> thin films prepared by RF magnetron sputtering. *Appl. Surf. Sci.* **2011**, *257*, 10869–10875. [[CrossRef](#)]
40. Wang, S.F.; Hsu, Y.F.; Lee, Y.S. Microstructural evolution and optical properties of doped TiO<sub>2</sub> films prepared by RF magnetron sputtering. *Ceram. Int.* **2006**, *32*, 121–125. [[CrossRef](#)]
41. Pradhan, S.S.; Sahoo, S.; Pradhan, S. Influence of annealing temperature on the structural, mechanical and wetting property of TiO<sub>2</sub> films deposited by RF magnetron sputtering. *Thin Solid Film.* **2010**, *518*, 6904–6908. [[CrossRef](#)]
42. Shen, Y.; Yu, H.; Yao, J.; Shao, S.; Fan, Z.; He, H.; Shao, J. Investigation on properties of TiO<sub>2</sub> thin films deposited at different oxygen pressures. *Opt. Laser Technol.* **2008**, *40*, 550–554. [[CrossRef](#)]
43. Chapman, B.N. Sputtering. In *Glow Discharge Processes—Sputtering and Plasma Etching*; Wiley: New York, NY, USA, 1980; pp. 177–296.



© 2019 by the authors. Licensee MDPI, Basel, Switzerland. This article is an open access article distributed under the terms and conditions of the Creative Commons Attribution (CC BY) license (<http://creativecommons.org/licenses/by/4.0/>).